

# Hydrogen bond donor-acceptor exchange in water

Jie Huang and Shibei Li\*

*Department of Physics, Wenzhou University, Wenzhou, Zhejiang 325035, China*

Gang Huang†

*Institute of Theoretical Physics, Chinese Academy of Sciences, Beijing 100190, China*

(Dated: May 26, 2022)

Water, the strangest liquid in the world, continues to astonish us despite centuries of research. Up until now, we have mainly been studying the static properties of water. Nevertheless, if we want to understand water, we have to watch the water molecules in motion. In the present study, we focus on one specific dynamic process: the donor-acceptor (DA) exchange, in which the Hydrogen (H-) bond donor reverses roles with the acceptor. We combined computer simulation and deep learning to study the dynamics of H-bonds between bulk water molecules. Using the *ab initio* molecular dynamics (AIMD) simulations, we observed DA exchange processes in bulk water. Then we designed a recurrent neural network (RNN) based model to classify different dynamic processes. Through this model, we found the ratio of DA exchanges to diffusion processes in bulk water is approximately 1:4 and hardly depends on temperatures from 280 to 360K. This result means that the DA exchange process in bulk water has a close and universal relationship with other dynamic processes.

## I. INTRODUCTION

As one of the big questions in the 21st century [1], the structure of water is essential for understanding cells, biological processes, and ecosystems [2–5]. Water’s surprising properties [6–8], such as increased density on melting, high surface tension, maximum density at 4°C, are closely related to the H-bond dynamics in water [9, 10]. However, few experimental studies can provide a molecular-level understanding of the dynamic properties of water [11], as it is tough to capture the ultrafast motion of atoms during dynamic processes [12]. Until now, we have mainly been studying the static properties of water. Nevertheless, watching water molecules as they dance is the key to understand the dynamic properties of water [13]. Many methods can be used to study water molecules’ motion, such as scanning tunneling microscopy (STM) [14, 15], infrared (IR) spectroscopy [12, 16–18], X-rays [13, 19, 20], neutron scattering [21], and computer simulations [22–24].

In the present study, we focus on one specific dynamic process: the donor-acceptor (DA) exchange process, in which the H-bond donor reverses roles with the acceptor in the same H-bond. The DA exchange process involves the quantum tunneling effect [15, 22, 24–26], which is essential for understanding water molecules’ dynamics. Also, since DA exchange processes are closely related to the H-bond network dynamics, it is likely to play a critical role in biological processes, like proton transfer [27–29]. So far, DA exchange processes have mainly been found in water dimer adsorbed on metal surfaces [15]. Using *ab initio* molecular dynamics (AIMD) simulations

[30], Ranea et al. [22] found that the DA exchange can be used to explain the rapid diffusion behavior of water dimer on the Pd(111) surface. Fang et al. [24] found that DA exchange is one mechanism of the rapid movement of water dimers on metal surfaces. As for bulk water, Lagge and Hynes found that the redirection of water molecules involves large-angle jumps [23], which involves the redirection of *multiple* water molecules referred to as *H-bond exchange*, and it is supported by the subsequent experiments [31, 32].

In addition to the above findings, although there are some simulation studies on the DA exchange process in water clusters [25, 26, 33, 34], as far as we know, the question of whether this process is present in bulk water has not been discussed. If it does present in bulk water, are there many of these processes compared to the other dynamic processes? To answer these questions, we simulated bulk water in a canonical (NVT) ensemble using AIMD simulations. We observed DA exchange processes in bulk water by analyzing the dynamic trajectory. To determine the proportion of DA exchange processes, we designed a recurrent neural network (RNN) based model to classify the H-bond dynamic processes. Using this model, we obtained the relative ratio of DA exchange and diffusion processes in bulk water and explored the effect of temperature on this ratio.

## II. RESULTS AND DISCUSSION

### A. Dynamic graph representation of H-bond networks

As shown in Fig. 1, a directed *dynamic graph* is used to describe the bulk water system of  $N$  water molecules. Each water molecule may form an H-bond with any of the remaining  $N-1$  molecules. For convenience, we call

\* shibenli@wzu.edu.cn

† hg08@lzu.edu.cn

any pair of water molecules ( $i, j$ ) a *quasi*-hydrogen bond (Q-bond), denoted as  $QB_{ij}$  and represented as a dashed line in Fig. 1. Inspired by Luzar and Chandler’s H-bond

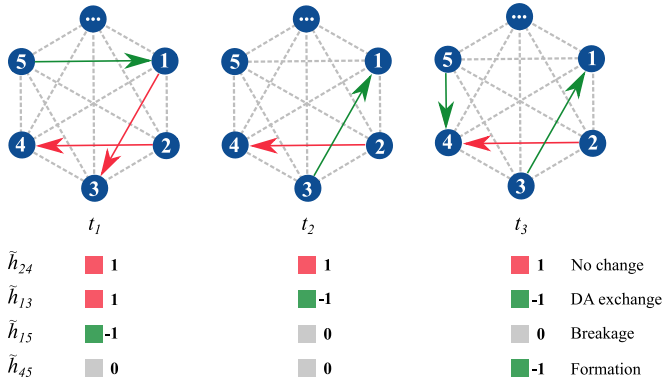


FIG. 1. Dynamic graph representation of the H-bond network in simulated bulk water. Nodes represent water molecules; solid red or green arrows represent H-bonds; and dashed grey lines represent Q-bonds. The colors red, grey, and green indicate  $\tilde{h}=1$ ,  $\tilde{h}=0$ , and  $\tilde{h}=-1$ , respectively. From the time sequence of  $\tilde{h}_{ij}$ , we know how the H-bond configuration of  $QB_{ij}$  changes over time. Four typical H-bond configuration change processes are illustrated for  $QB_{24}$ ,  $QB_{13}$ ,  $QB_{15}$ , and  $QB_{45}$ , corresponding to no change, DA exchange, breakage, and formation, respectively.

population operator [11], we define a *directed* H-bond population operator  $\tilde{h}_{ij}$  for  $QB_{ij}$  ( $i < j$ ) at time  $t$  as Eq. 1. We know from  $\tilde{h}_{ij}$  whether an H-bond exists in

$$\tilde{h}_{ij}(t) = \begin{cases} 1 & \text{H-bonded, } i \text{ is the donor} \\ 0 & \text{Not H-bonded} \\ -1 & \text{H-bonded, } j \text{ is the donor} \end{cases} \quad (1)$$

$QB_{ij}$  and the donor-acceptor pair of the formed H-bond. At the bottom of Fig. 1, we demonstrate four typical H-bond configuration change processes: no change, DA exchange, breakage, and formation. Therefore, the time sequence of  $\tilde{h}$  can be used to simplify the description of the H-bond dynamics. Besides, the Q-bonds likely to form H-bonds are the most relevant water pairs to the breakage and reforming of H-bond networks. The following geometric criteria [35–37] of an H-bond is used:  $R_{OO'} < R_{\text{cutoff}} = 3.5 \text{ \AA}$ ,  $\widehat{\text{DHA}} > \theta_{\text{cutoff}} = 120^\circ$ , where  $R_{OO'}$  is the O-O distance, and  $\widehat{\text{DHA}}$  is the O-H $\cdots$ O angle. As shown in Fig. 2,  $R_{OO'}$ ,  $\theta_a$ ,  $\theta_b$ ,  $\theta_c$ , and  $\theta_d$  are monitored for Q-bonds to study the reorientation and diffusion mechanism of H-bonds.

## B. Donor-acceptor exchange process

The AIMD simulation trajectory allows us to observe the details of the H-bond dynamics. Figure 3 demonstrates the dynamics of the distance, angles, and directed

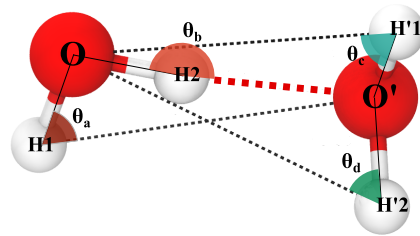


FIG. 2. Scheme of the geometric coordinates.  $R_{OO'}$  is the O-O distance. Four angles  $\widehat{\text{OH1O'}}$ ,  $\widehat{\text{OH2O'}}$ ,  $\widehat{\text{O'H'1O}}$ , and  $\widehat{\text{O'H'2O}}$  are represented as  $\theta_a$ ,  $\theta_b$ ,  $\theta_c$ , and  $\theta_d$ , respectively. If  $R_{OO'} < 3.5 \text{ \AA}$ , and any angle  $\theta > 120^\circ$  ( $\theta \in \{\theta_a, \theta_b, \theta_c, \theta_d\}$ ), then an H-bond exists in this Q-bond. Here, the oxygen atom O as a donor donates the hydrogen atom H2 to the acceptor O'. Since  $R_{OO'} < 3.5 \text{ \AA}$  and  $\theta_b > 120^\circ$ , we describe this state of  $QB_{OO'}$  at this time  $t$  by  $\tilde{h}_{OO'}(t) = 1$ .

H-bond population operator for  $QB_{OO'}$ . Intervals  $I_1$ ,  $I_2$ , and  $I_3$  correspond to three typical H-bond dynamic processes. *DA exchange* ( $I_1$ ): We notice  $\theta_b > \theta_{\text{cutoff}}$  in the first half and  $\theta_d > \theta_{\text{cutoff}}$  in the second half. Besides,  $\tilde{h}_{OO'}$  changes from 1 to  $-1$ , indicating the donor and acceptor have exchanged. *Translational diffusion* ( $I_2$ ):  $\tilde{h}_{OO'} = -1$  in the first half of  $I_2$ , and  $\tilde{h}_{OO'} = 0$  for most of the second half. There is no H-bond in the second half because  $R_{OO'} > R_{\text{cutoff}}$ , i.e., the increase of distance  $R_{OO'}$  causes the H-bond to break. *HH exchange* ( $I_3$ ): At first, the hydrogen atom H'1 is donated to form an H-bond as  $\theta_c > \theta_{\text{cutoff}}$ . Then  $\theta_c$  decreases and  $\theta_d$  increases until  $\theta_d > \theta_{\text{cutoff}}$ , i.e., the other hydrogen atom H'2 of the donor is donated to form the H-bond. Therefore, the hydrogen atom contributed by the donor is changed. Because of the identity of hydrogen atoms, it is impossible to distinguish the configuration of water molecules before and after the HH exchange. However, during the DA exchange process, the direction of the water molecules’ dipole moment will change, indicating the water molecules’ microscopic configuration will change. So in the rest of this article, we focus on the DA exchange process.

Figure 4 shows a typical DA exchange process in bulk water (see Fig. S5 and movies S1-S2 in SI Appendix for more H-bond configuration change processes). A dashed line represents an H-bond, and its color (red or green) indicates its “direction.” Using  $\tilde{h}$ , we can describe the H-bond configuration change progress without paying attention to the distance and angles. Therefore,  $\tilde{h}$  dramatically simplifies the description for the H-bond configuration change process. Nevertheless, during dynamic processes, the value of  $\tilde{h}$  would fluctuate due to the vibration of water molecules, which will bring a huge challenge for the classification of H-bond configuration change processes. Next, we will discuss how to use a deep learning based method to classify H-bond configuration change processes and find the proportion of DA exchange in the dynamics of water molecules in bulk water.

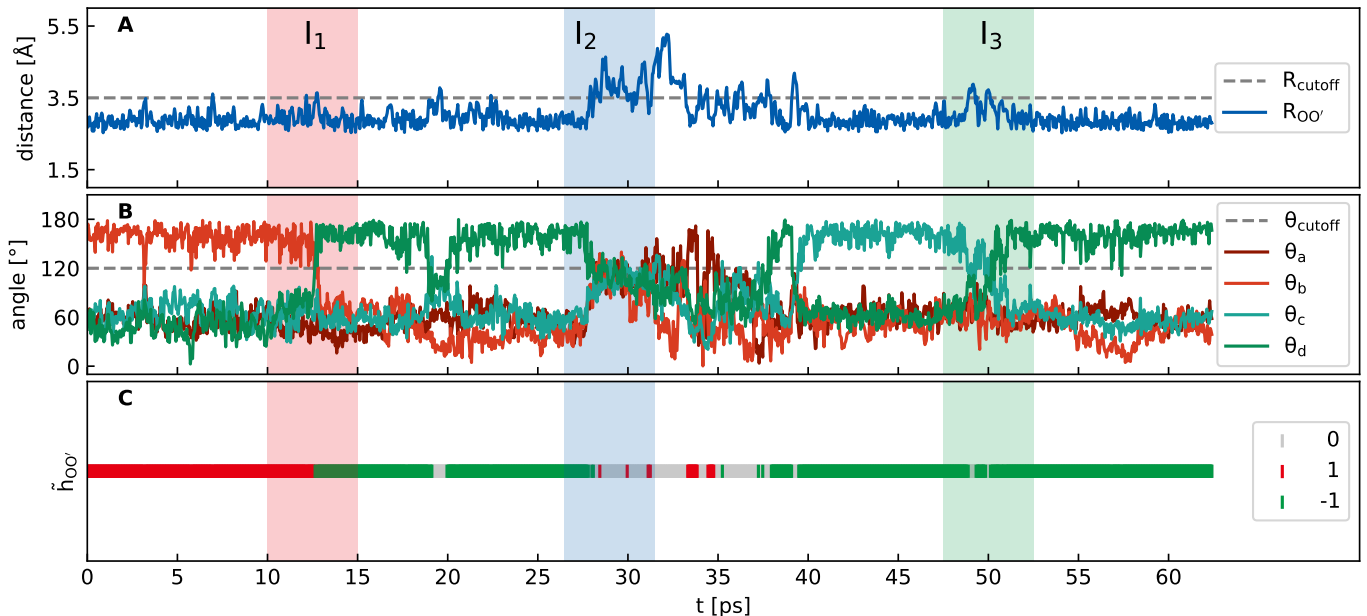


FIG. 3. DA exchange ( $I_1$ ), diffusion ( $I_2$ ), and HH exchange ( $I_3$ ) process for one typical Q-bond in bulk water. When an H-bond exists in a Q-bond if  $\theta_a > \theta_{\text{cutoff}}$  or  $\theta_b > \theta_{\text{cutoff}}$ , then the oxygen atom O is the donor; else, if  $\theta_c > \theta_{\text{cutoff}}$  or  $\theta_d > \theta_{\text{cutoff}}$ , then the oxygen atom O' is the donor. Three typical processes are DA exchange, where the water pairs exchange their roles as H-bond donor and acceptor; diffusion, where the H-bond is breaking as the distance increase of this water pair; and HH exchange, where the donated hydrogen atom of the H-bond donor exchanged. Through  $\tilde{h}$ , we can see whether an H-bond exists between a Q-bond, also know the donor and acceptor if an H-bond exists. In panel (C), the grey, red, and green lines indicate the  $\tilde{h}'_{\text{OO}}$  states.

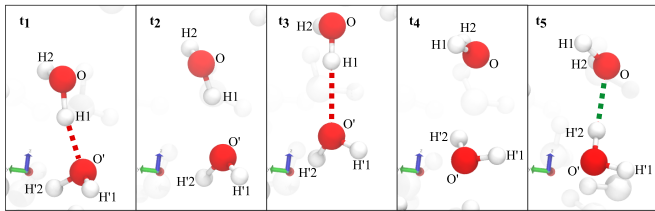


FIG. 4. A typical DA exchange process, where the two water molecules exchange their roles as H-bond donor and acceptor via water molecules' reorientation in a concerted manner. The donor oxygen atom has changed from the original O to O'. Besides, we have also noticed that the H-bond briefly breaks during the DA exchange process, causing the fluctuation of the  $\tilde{h}$  sequence.

### C. RNN based classifier for H-bond configuration change process

We can see the DA exchange and diffusion processes intuitively from  $\tilde{h}$ . Specifically, in the DA exchange process,  $\tilde{h}$  changes from  $\pm 1$  to  $\mp 1$ ; in the diffusion process,  $\tilde{h}$  changes from  $\pm 1$  to 0. Therefore, in principle, by observing the sequence of  $\tilde{h}$  within a time window, we can classify the H-bond configuration changes during this period. Although we can see some change patterns in DA exchange and diffusion processes, it is still challenging to distinguish different  $\tilde{h}$  sequences due to the fluctua-

tion. Therefore, we have designed a processing flow to classify the H-bond configuration change process based on RNN, as shown in Fig. 5. In the preprocessor, we use a low-pass filter to filter out the high-frequency fluctuations of  $\tilde{h}$  sequences. As we focus on the configuration change processes of H-bonds, we exclude sequences that do not have an H-bond at the beginning ( $T_1$ ) and the sequences whose H-bond configuration do not change ( $T_2$ ,  $T_3$ ) according to the initial value and the variance of  $\tilde{h}$  sequences (see Materials and Methods). After preprocessing, the task we need to deal with is a non-trivial time series classification problem: In addition to DA exchange and diffusion processes, there are also many irregular and complicated processes. We call the sequences of DA exchange and diffusion *positive* and all sequences other than these two types *negative* for convenience. Negative sequences ( $T_4$ ) do not have any particular pattern. We do not expect that general supervised learning can be used to distinguish them. Nevertheless, we can teach a machine to learn to *recognize* positive sequences. Due to the need to classify time series, we use a typical method for modeling ordered data [38–40], recurrent neural network (RNN) [41, 42]. Specifically, we have designed a bidirectional long short-term memory (BLSTM) autoencoder (AE) and trained this model using positive sequences (see Fig. S2 in SI Appendix for BLSTM AE structure). After training, the autoencoder can reconstruct positive processes very well. Then we input negative sequences

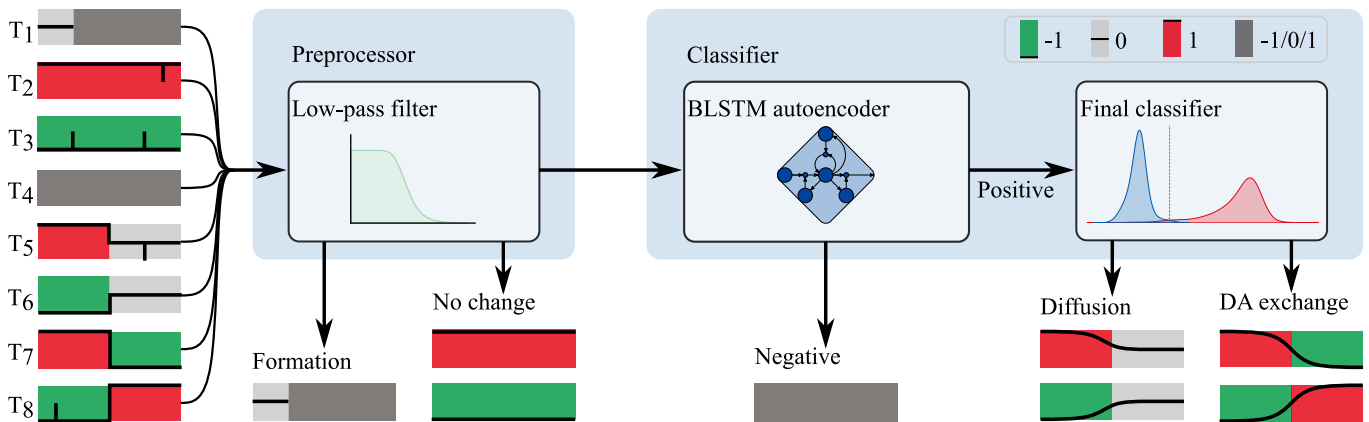


FIG. 5. The processing flow of the H-bond configuration change classifier based on RNN. (i). Different types of  $\tilde{h}$  sequences: T<sub>1</sub>: Formation or no H-bond; T<sub>2</sub>, T<sub>3</sub>: No change; T<sub>4</sub>: Negative sequence hard to be classified; T<sub>5</sub>, T<sub>6</sub>: Diffusion; T<sub>7</sub>, T<sub>8</sub>: DA exchange. We refer to the sequences of diffusion and DA exchange as positive sequences. (ii). The preprocessor filters out the high-frequency components of  $\tilde{h}$  and excludes T<sub>1</sub>, T<sub>2</sub>, and T<sub>3</sub>. (iii). The classifier consists of a bidirectional LSTM autoencoder (BLSTM AE) to separate the positive and negative sequences and a final classifier to distinguish diffusion and DA exchange.

into the autoencoder. Likely, it would not be able to reconstruct them well, leading to the reconstruction errors of these negative sequences greater than that of the positive sequences. Through the reconstruction error, we can determine whether a  $\tilde{h}$  sequence is positive or negative. Finally, we use a *final classifier* to distinguish between

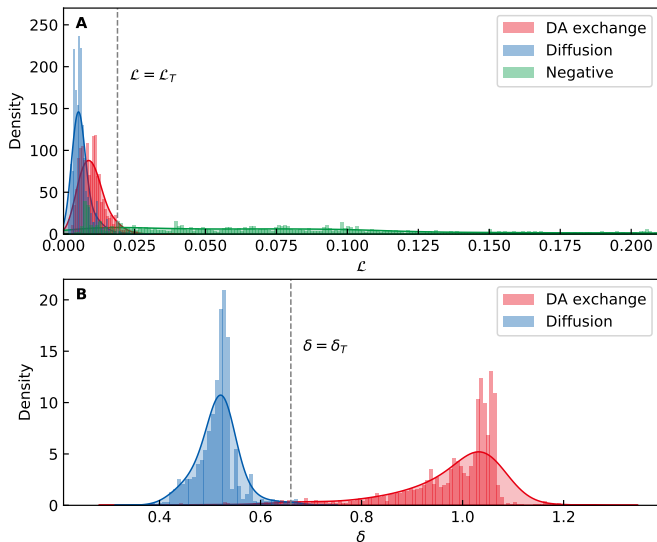


FIG. 6. (A) Densities of reconstruction error  $\mathcal{L}$  for DA exchange, diffusion, and negative sequences. (i) BLSTM AE can reconstruct positive sequences well. Hence, the reconstruction errors for DA exchange and diffusion sequences are relatively small, mainly less than  $\mathcal{L}_T$ . (ii) Since negative sequences are not used to train BLSTM AE, it is much more difficult for the autoencoder to reconstruct them. Therefore, the reconstruction errors are relatively large, mainly greater than  $\mathcal{L}_T$ . (iii) Once  $\mathcal{L}_T$  is determined, we use it as the threshold to distinguish positive and negative sequences. (B) Densities of the range  $\delta$  for DA exchange and diffusion sequences. The two densities are significantly different from each other.

DA exchange and diffusion processes from positive sequences. We use the range of a positive sequence  $\mathbf{x}$  to determine whether it is DA exchange or diffusion, which is defined as  $\delta(\mathbf{x}) = \max \mathbf{x} - \min \mathbf{x}$ .

Figure 6 (A) shows the densities of the reconstruction errors for DA exchange, diffusion, and negative sequences. Since BLSTM AE can reconstruct positive sequences well, the reconstruction errors of DA exchange and diffusion sequences are small, most of which are smaller than the reconstruction error threshold  $\mathcal{L}_T$  ( $\mathcal{L}_T$  is determined in SI Appendix, Fig. S3). Negative sequences are not used to train the autoencoder, so it is much more difficult to reconstruct them. Hence, the reconstruction errors are relatively large, most of which are greater than  $\mathcal{L}_T$ . As long as we find a suitable reconstruction error threshold, we can get a classifier for positive and negative sequences. Figure 6 (B) shows the densities for the range of normalized DA exchange and diffusion sequences. The two distributions are significantly different from each other. Therefore, the final classifier can distinguish DA exchange and diffusion very well via  $\delta_T = 0.66$ , as shown in the dashed line (see the classification process in SI Appendix, Fig. S5-S6). Therefore, we have obtained an H-bond configuration change classifier based on an RNN autoencoder. Next, we will use this model to explore the relative proportion of DA exchange at different temperatures.

#### D. Proportions of DA exchange at different temperatures

To explore the effect of temperature on the H-bond configuration change process, we have simulated nine bulk water systems containing 64 water molecules. The temperature ranges from 280 to 360K every 10K. Using the RNN based model, we classify  $\tilde{h}$  sequence, count

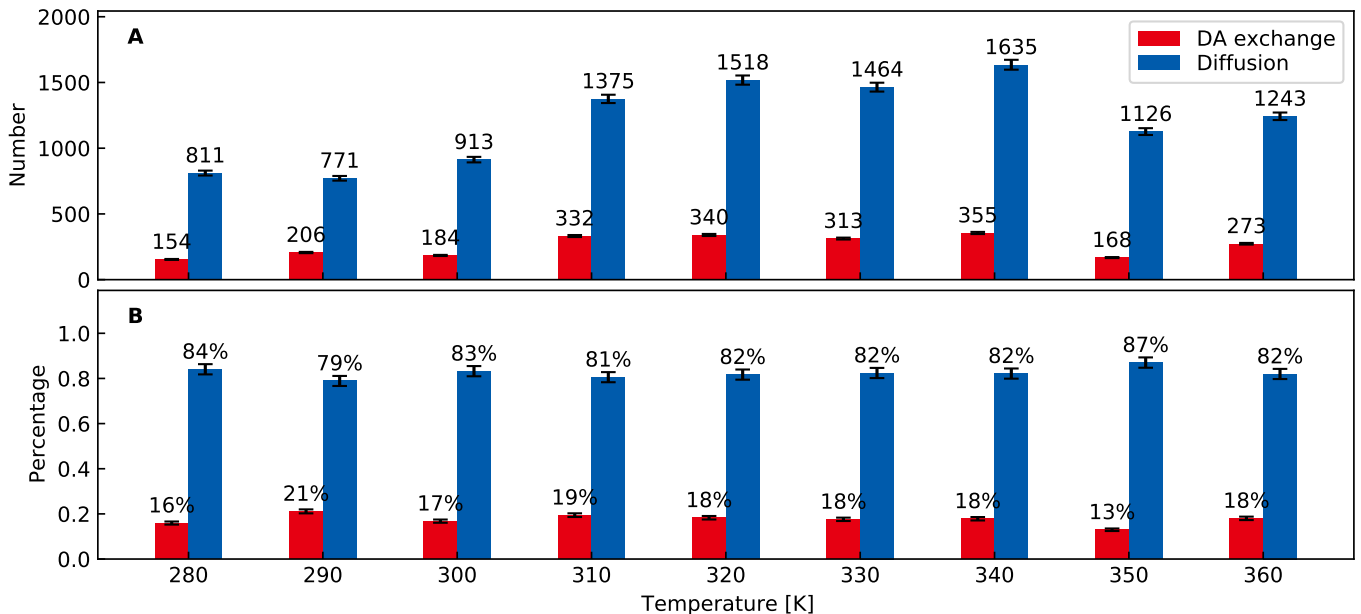


FIG. 7. The number (A) and proportion (B) of DA exchange and diffusion processes determined by the RNN based classifier at different temperatures. (i) With the temperature increasing, the number of DA exchange and diffusion processes increases first and then decreases on the whole. (ii) The relative ratio of DA exchange to diffusion basically does not depend on temperature.

the number of DA exchange and diffusion sequences at each temperature. As shown in Fig. 7, the number of DA exchange and diffusion processes shows a ‘rising first, then decreasing’ trend as the temperature increases. In other words, there is an overall upward trend from 280 to 330K. However, as the temperature continues to rise, the number of DA exchange and diffusion processes tends to decrease. On the other hand, although the statistics of the number of DA exchange and diffusion processes vary at different temperatures, the relative ratios between the two are almost unchanged, which is still about 1:4. This result indicates that the relative ratio is almost not dependent on temperature, and the DA exchange process is another important mechanism in bulk water besides the diffusion process. Next, we will explain this trend of the number of DA exchange and diffusion processes from the following two aspects: the number of H-bond per molecule and the change rate of the coarse-grained H-bond network configuration.

#### E. The number of H-bonds per molecule and the number of the coarse-grained H-bond network configuration per unit time

To understand the trend in Fig. 7 (A), we first calculate the number of H-bonds per molecule ( $n_{\text{HB}}$ ) in the simulated system. At time  $t$ ,  $n_{\text{HB}}$  can be expressed as Eq. 2.

$$n_{\text{HB}}(t) = \frac{2}{N} \sum_{i=1}^N \sum_{j>i}^N |\tilde{h}_{ij}(t)| \quad (2)$$

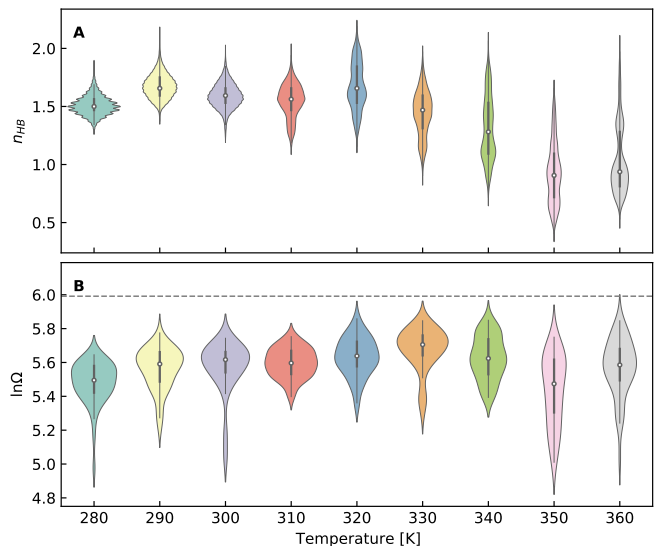


FIG. 8. The temperature dependence of (A) The distributions of the number  $n_{\text{HB}}$  of H-bonds per molecule. (B) The distributions of  $\ln \Omega$  characterizing the rate of H-bond breakage and reforming (Observation time  $t_w = 1$  ps).

At a certain temperature, by counting  $n_{\text{HB}}$  at different simulation times (frames), we get the distribution of  $n_{\text{HB}}$  at different values for this temperature (one density plot in Fig. 8 A). Then we use an  $L$ -dimensional vector  $\tilde{\mathbf{h}}(t)$  to represent the coarse-grained H-bond network *configuration* for the simulated bulk water system at time  $t$  in

Eq. 3,

$$\tilde{\mathbf{h}}(t) = (\tilde{h}_{12}(t), \tilde{h}_{13}(t), \dots, \tilde{h}_{ij}(t), \dots, \tilde{h}_{N-1,N}(t)) \quad (3)$$

where  $L = N(N - 1)/2$  is the number of Q-bonds in the system. So in a unit time, we get a set  $H$  of  $\tilde{\mathbf{h}}(t)$  in Eq. 4,

$$H = \{\tilde{\mathbf{h}}(t) \mid t = t_0 + k\Delta t, k \in \{0, 1, \dots, M\}\} \quad (4)$$

where  $t_0$  represents the start time of the observation window,  $\Delta t$  is the time interval between two adjacent frames, and  $M$  is a parameter to control the length of the unit time window. In a unit time  $t_w = M\Delta t$ , the number of graph configuration can be expressed as  $\Omega = |H|$ , where  $|H|$  is the size of the set  $H$ , i.e., the number of different vector  $\tilde{\mathbf{h}}$  in  $H$ . The number  $\Omega$  of graph configuration per unit time characterizes the *rate* of breakage and reforming of the H-bonds in bulk water. The theoretical maximum value of  $\Omega$  in  $t_w$  is  $M + 1$ ; in this case, all  $\tilde{\mathbf{h}}$ s are different. By changing the starting point  $t_0$ , we get the distribution of  $\Omega$ .

Figure 8 shows the temperature dependence of the distributions of  $n_{\text{HB}}$  and  $\ln \Omega$ . From the medians (white dots) of violin plots in Fig. 8 (B), we see  $\Omega$  is relatively smaller at lower temperatures, indicating fewer changes of H-bond configuration in bulk water. This explains why the total number of DA exchange and diffusion processes at lower temperatures in Fig. 7 (A) are small. Besides, the direct reason for the decrease in the number of DA exchange and diffusion processes is that  $n_{\text{HB}}$  decreases with increasing temperature. Therefore, the number of DA exchange and diffusion processes in Fig. 7 (A) is determined by  $n_{\text{HB}}$  and  $\Omega$  together. Moreover, the temperature dependence of the relaxation time is consistent with that of the average number of H-bonds per molecule (SI Appendix, Fig. S7); and the vibrational density of states (VDOS) of water molecules at higher temperatures have a blue-shift OH-stretching band (SI Appendix, Fig. S8). These results are also consistent with the above conclusion that  $n_{\text{HB}}$  decreases as temperature increases.

## F. Conclusions

(i) In this work, unlike focusing on the H-bonds switching between multiple water molecules in the large-angle jump model, we keep our eyes on water pairs (Q-bond) in bulk water. We observed two water molecules cooperate to complete the DA exchange process via concerted rearrangement by monitoring the O-O distance and angles. Besides, large-angle changes are also observed in these processes from the Q-bond's angle dynamics, indicating the DA exchange process is consistent with the jump model from another perspective. (ii) The relative ratio of DA exchange and diffusion processes is approximately 1:4. This ratio hardly depends on temperature from 280 to 360K, indicating that the DA exchange process in bulk water has a close and universal relationship

with other dynamic processes. (iii) To determine the relative proportion of DA exchange processes, we use the dynamic graph and newly defined directed H-bond population operator to model water systems. By analyzing the time series of  $\tilde{\mathbf{h}}$ , we can see the H-bond dynamics between water pairs. This reasonable coarse-grained description of the H-bond network simplifies the analysis of H-bond dynamics dramatically. Besides, the BLSTM AE is used to successfully classify different types of  $\tilde{\mathbf{h}}$  sequences, indicating the great potential to use RNN based deep learning methods to understand more complex dynamic processes in water.

## III. MATERIALS AND METHODS

### A. AIMD simulations

AIMD simulations were carried out for bulk water of 64 water molecules within the canonical NVT ensemble using CP2K/QUICKSTEP (v7.1) [43]. The length of the periodic cubic box was 12.4295 Å. The discretized integration time step  $\Delta t$  was set to 0.5 fs. The simulation time was 60 ps. The BLYP functional, which consists of Becke non-local exchange [44] and Lee-Yang-Parr correlation [45], was used; Interactions between the valence electrons and the ionic cores were described by GTH pseudopotentials [46, 47]; Valence electrons were expanded in a basis set consisting of double-zeta Gaussian functions [48] and plane waves with a cutoff energy of 280 Ry [43]. The Nosé-Hoover chain thermostat [49] was used to conserve temperature. DFT-D3 correction [50] for the dispersion interaction was used to obtain an accurate description of the vibrational properties.

### B. Sequence collection and preprocessing

By observing the dynamics of O-O distance, angles, and directed H-bond population operator of Q-bonds, we collected the sequences of DA exchange and diffusion process (SI Appendix, Fig. S5 (A)-(F)). The sequence length of  $\tilde{\mathbf{h}}$  was 200 corresponding to a 8 ps time window. Positive sequences in which only one DA exchange or diffusion process occurred were collected. Negative  $\tilde{\mathbf{h}}$  sequences used to evaluate the BLSTM AE classifier were also collected. BLSTM AE was trained by 6786 positive sequences, of which the DA exchange and diffusion processes each accounted for half (754 positive sequences at each temperature). There were 18,931 negative sequences for evaluating the BLSTM AE classifier. The second-order Butterworth filter was implemented using Signal module in Scipy [51]. After processing, the filtered sequence  $\tilde{h}_f[n]$  was obtained. In addition, two parameters  $\alpha_T = 0.15$ ,  $\sigma_T = 0.1$  were used to exclude the formation sequences and inertial sequences. If  $\tilde{h}_f[0] - 0.5 < \alpha_T$ , indicating no H-bond at the beginning ( $T_1$ ). If the stan-

dard deviation  $\sigma$  of  $\tilde{h}_f[n]$  satisfy  $\sigma < \sigma_T$ , then we consider the H-bond configuration in the Q-bond has not changed ( $T_2$ ,  $T_3$ ).

### C. Bidirectional LSTM autoencoder

Combining LSTM units, bidirectional network structure, and autoencoder, we obtained a bidirectional LSTM autoencoder (BLSTM AE). The BLSTM AE consists of two parts, the encoder and the decoder, which can be expressed as two transformations,  $\phi : \mathcal{X} \rightarrow \mathcal{F}$  and  $\psi : \mathcal{F} \rightarrow \mathcal{X}$ , where  $\mathcal{X}$  and  $\mathcal{F}$  are the input space and the feature space, respectively. The dimension of  $\mathcal{F}$  is smaller than that of  $\mathcal{X}$ , and the feature vector  $\phi(\mathbf{x})$  is the compressed representation of input  $\mathbf{x}$ . The input  $\mathbf{x}$  of BLSTM AE is the normalized and filtered directed H-bond population operator sequence  $\tilde{h}_f[n]$ . The reconstruction error of BLSTM AE for a sequence  $\mathbf{x} = \tilde{h}_f[n]$  is defined as

$$\mathcal{L}_{\omega, \omega'}(\mathbf{x}) = \|\mathbf{x} - \psi_{\omega'}(\phi_{\omega}(\mathbf{x}))\|^2 \quad (5)$$

where  $\omega, \omega'$  represent the parameters of the encoder and decoder respectively. The purpose of training is to obtain the optimal  $\omega, \omega'$ ,

$$\omega^*, \omega'^* = \arg \min_{\omega, \omega'} \frac{1}{m} \sum_{i=1}^m \mathcal{L}_{\omega, \omega'}(\mathbf{x}^i) \quad (6)$$

where  $\mathbf{x}^i$  represents the  $i$ -th sequence (SI Appendix, Fig. S1-S2).

### ACKNOWLEDGMENTS

This research was supported by the National Natural Science Foundation of China (NSFC) (Grant Nos. 21973070). The simulations were performed on the cluster in the College of Mathematics and Physics at Wenzhou University.

### DATA AVAILABILITY STATEMENT

The data that support the findings of this study are available from the corresponding author upon reasonable request.

- 
- [1] D. Kennedy, What don't we know?, *Science* **309**, 75 (2005).
- [2] F. Franks, *Water: a matrix of life*, 2nd ed. (Royal Society of Chemistry, 2000).
- [3] S. K. Pal and A. H. Zewail, Dynamics of water in biological recognition, *Chemical Reviews* **104**, 2099 (2004).
- [4] M. Chaplin, Do we underestimate the importance of water in cell biology?, *Nature Reviews Molecular Cell Biology* **7**, 861 (2006).
- [5] P. Ball, Water is an active matrix of life for cell and molecular biology, *Proceedings of the National Academy of Sciences* **114**, 13327 (2017).
- [6] F. H. Stillinger, Water revisited, *Science* **209**, 451 (1980).
- [7] J. R. Errington and P. G. Debenedetti, Relationship between structural order and the anomalies of liquid water, *Nature* **409**, 318 (2001).
- [8] I. Dumé, Second critical point appears in two models of water, *Physics World* **33**, 7i (2020).
- [9] A. Nilsson and L. G. M. Pettersson, The structural origin of anomalous properties of liquid water, *Nature Communications* **6**, 10.1038/ncomms9998 (2015).
- [10] U. Wilhelmsen and D. Deutsches Elektronen-Synchrotron, *The strangest liquid in the world: water amazes scientists time and again*, edited by T. Mundzeck, Vol. 20 (Deutsches Elektronen Synchrotron, DESY, Hamburg, 2020) p. 44 pages.
- [11] A. Luzar and D. Chandler, Hydrogen-bond kinetics in liquid water, *Nature* **379**, 55 (1996).
- [12] E. T. Karamatskos, S. Raabe, T. Mullins, A. Trabatttoni, P. Stammer, G. Goldsztejn, R. R. Johansen, K. Długołeki, H. Stapelfeldt, M. J. J. Vrakking, S. Tripel, A. Rouzée, and J. Küpper, Molecular movie of ultrafast coherent rotational dynamics of OCS, *Nature Communications* **10**, 10.1038/s41467-019-11122-y (2019).
- [13] F. Perakis, G. Camisasca, T. J. Lane, A. Späh, K. T. Wikfeldt, J. A. Sellberg, F. Lehmkuhler, H. Pathak, K. H. Kim, K. Amann-Winkel, S. Schreck, S. Song, T. Sato, M. Sikorski, A. Eilert, T. McQueen, H. Ogasawara, D. Nordlund, W. Roseker, J. Koralek, S. Nelson, P. Hart, R. Alonso-Mori, Y. Feng, D. Zhu, A. Robert, G. Grübel, L. G. M. Pettersson, and A. Nilsson, Coherent x-rays reveal the influence of cage effects on ultrafast water dynamics, *Nature Communications* **9**, 10.1038/s41467-018-04330-5 (2018).
- [14] T. Mitsui, Water diffusion and clustering on pd(111), *Science* **297**, 1850 (2002).
- [15] T. Kumagai, M. Kaizu, S. Hatta, H. Okuyama, T. Aruga, I. Hamada, and Y. Morikawa, Direct observation of hydrogen-bond exchange within a single water dimer, *Physical Review Letters* **100**, 10.1103/physrevlett.100.166101 (2008).
- [16] H. J. Bakker and H.-K. Nienhuys, Delocalization of protons in liquid water, *Science* **297**, 587 (2002).
- [17] C. J. Fecko, Ultrafast hydrogen-bond dynamics in the infrared spectroscopy of water, *Science* **301**, 1698 (2003).
- [18] K. ichi Inoue, M. Ahmed, S. Nihonyanagi, and T. Tahara, Reorientation-induced relaxation of free OH at the air/water interface revealed by ultrafast heterodyne-detected nonlinear spectroscopy, *Nature Communications* **11**, 10.1038/s41467-020-19143-8 (2020).
- [19] T. Iwashita, B. Wu, W.-R. Chen, S. Tsutsui, A. Q. R. Baron, and T. Egami, Seeing real-space dynamics of liq-

- uid water through inelastic x-ray scattering, *Science Advances* **3**, e1603079 (2017).
- [20] Z.-H. Loh, G. Doumy, C. Arnold, L. Kjellsson, S. H. Southworth, A. A. Haddad, Y. Kumagai, M.-F. Tu, P. J. Ho, A. M. March, R. D. Schaller, M. S. B. M. Yusof, T. Debnath, M. Simon, R. Welsch, L. Inhester, K. Khalili, K. Nanda, A. I. Krylov, S. Moeller, G. Coslovich, J. Koralek, M. P. Minitti, W. F. Schlotter, J.-E. Rubensson, R. Santra, and L. Young, Observation of the fastest chemical processes in the radiolysis of water, *Science* **367**, 179 (2020).
- [21] T. Head-Gordon and G. Hura, Water structure from scattering experiments and simulation, *Chemical Reviews* **102**, 2651 (2002).
- [22] V. A. Ranea, A. Michaelides, R. Ramírez, P. L. de Andres, J. A. Vergés, and D. A. King, Water dimer diffusion on  $\text{pd}\{111\}$  assisted by an h-bond donor-acceptor tunneling exchange, *Physical Review Letters* **92**, 10.1103/physrevlett.92.136104 (2004).
- [23] D. Laage and J. T. Hynes, A Molecular Jump Mechanism of Water Reorientation, *Science* **311**, 832 (2006).
- [24] W. Fang, J. Chen, P. Pedevilla, X.-Z. Li, J. O. Richardson, and A. Michaelides, Origins of fast diffusion of water dimers on surfaces, *Nature Communications* **11**, 10.1038/s41467-020-15377-8 (2020).
- [25] R. S. Fellers, C. Leforestier, L. B. Braly, M. G. Brown, and R. J. Saykally, Spectroscopic determination of the water pair potential, *Science* **284**, 945 (1999).
- [26] F. N. Keutsch and R. J. Saykally, Water clusters: Untangling the mysteries of the liquid, one molecule at a time, *Proceedings of the National Academy of Sciences* **98**, 10533 (2001).
- [27] N. Agmon, The grotthuss mechanism, *Chemical Physics Letters* **244**, 456 (1995).
- [28] J. L. Thomaston, R. A. Woldeyes, T. Nakane, A. Yamashita, T. Tanaka, K. Koiwai, A. S. Brewster, B. A. Barad, Y. Chen, T. Lemmin, M. Uervirojnangkoorn, T. Arima, J. Kobayashi, T. Masuda, M. Suzuki, M. Sugahara, N. K. Sauter, R. Tanaka, O. Nureki, K. Tono, Y. Joti, E. Nango, S. Iwata, F. Yumoto, J. S. Fraser, and W. F. DeGrado, XFEL structures of the influenza m2 proton channel: Room temperature water networks and insights into proton conduction, *Proceedings of the National Academy of Sciences* **114**, 13357 (2017).
- [29] M. D. Gelenter, V. S. Mandala, M. J. M. Niesen, D. A. Sharon, A. J. Dregni, A. P. Willard, and M. Hong, Water orientation and dynamics in the closed and open influenza b virus m2 proton channels, *Communications Biology* **4**, 338 (2021).
- [30] T. D. Kühne, M. Iannuzzi, M. D. Ben, V. V. Rybkin, P. Seewald, F. Stein, T. Laino, R. Z. Khatullin, O. Schütt, F. Schiffmann, D. Golze, J. Wilhelm, S. Chulkov, M. H. Bani-Hashemian, V. Weber, U. Borštnik, M. TAILLEFUMIER, A. S. Jakobovits, A. Lazaro, H. Pabst, T. Müller, R. Schade, M. Guidon, S. Andermatt, N. Holmberg, G. K. Schenter, A. Hehn, A. Bussy, F. Belleflamme, G. Tabacchi, A. Glöß, M. Lass, I. Bethune, C. J. Mundy, C. Plessl, M. Watkins, J. Vandevondele, M. Krack, and J. Hutter, CP2k: An electronic structure and molecular dynamics software package - quickstep: Efficient and accurate electronic structure calculations, *The Journal of Chemical Physics* **152**, 194103 (2020).
- [31] D. E. Moilanen, D. Wong, D. E. Rosenfeld, E. E. Fenn, and M. D. Fayer, Ion-water hydrogen-bond switching observed with 2d ir vibrational echo chemical exchange spectroscopy, *Proceedings of the National Academy of Sciences* **106**, 375 (2009).
- [32] M. Ji, M. Odellius, and K. J. Gaffney, Large angular jump mechanism observed for hydrogen bond exchange in aqueous perchlorate solution, *Science* **328**, 1003 (2010).
- [33] R. Schulz, Y. von Hansen, J. O. Daldrop, J. Kappler, F. Noé, and R. R. Netz, Collective hydrogen-bond rearrangement dynamics in liquid water, *The Journal of Chemical Physics* **149**, 244504 (2018).
- [34] E. Méndez and D. Laria, Nuclear quantum effects on the hydrogen bond donor-acceptor exchange in water-water and water-methanol dimers, *The Journal of Chemical Physics* **153**, 054302 (2020).
- [35] F. Sciortino and S. L. Fornili, Hydrogen bond cooperativity in simulated water: Time dependence analysis of pair interactions, *The Journal of Chemical Physics* **90**, 2786 (1989).
- [36] S. Balasubramanian, S. Pal, and B. Bagchi, Hydrogen-bond dynamics near a micellar surface: Origin of the universal slow relaxation at complex aqueous interfaces, *Physical Review Letters* **89**, 10.1103/physrevlett.89.115505 (2002).
- [37] N. Michaud-Agrawal, E. J. Denning, T. B. Woolf, and O. Beckstein, MDAnalysis: A toolkit for the analysis of molecular dynamics simulations, *Journal of Computational Chemistry* **32**, 2319 (2011).
- [38] T. W. Hughes, I. A. D. Williamson, M. Minkov, and S. Fan, Wave physics as an analog recurrent neural network, *Science Advances* **5**, 10.1126/sciadv.aay6946 (2019).
- [39] N. Rank, B. Pfahringer, J. Kempfert, C. Stamm, T. Kühne, F. Schoenrath, V. Falk, C. Eickhoff, and A. Meyer, Deep-learning-based real-time prediction of acute kidney injury outperforms human predictive performance, *npj Digital Medicine* **3**, 10.1038/s41746-020-00346-8 (2020).
- [40] S.-T. Tsai, E.-J. Kuo, and P. Tiwary, Learning molecular dynamics with simple language model built upon long short-term memory neural network, *Nature Communications* **11**, 10.1038/s41467-020-18959-8 (2020).
- [41] J. J. Hopfield, Neural networks and physical systems with emergent collective computational abilities, *Proceedings of the National Academy of Sciences* **79**, 2554 (1982).
- [42] S. Hochreiter and J. Schmidhuber, Long short-term memory, *Neural Computation* **9**, 1735 (1997).
- [43] J. Vandevondele, M. Krack, F. Mohamed, M. Parrinello, T. Chassaing, and J. Hutter, Quickstep: Fast and accurate density functional calculations using a mixed gaussian and plane waves approach, *Comput. Phys. Commun.* **167**, 103 (2005).
- [44] A. D. Becke, Density-functional exchange-energy approximation with correct asymptotic behavior, *Phys. Rev. A* **38**, 3098 (1988).
- [45] C. Lee, W. Yang, and R. G. Parr, Development of the colic-salvetti correlation-energy formula into a functional of the electron density, *Phys. Rev. B* **37**, 785 (1988).
- [46] C. Hartwigsen, S. Goedecker, and J. Hutter, Relativistic separable dual-space gaussian pseudopotentials from H to Rn, *Phys. Rev. B* **58**, 3641 (1998).
- [47] J. H. G. Lippert and M. Parrinello, The gaussian and augmented-plane-wave density functional method for ab

- initio molecular dynamics simulations, *Theor. Chem. Acc.* **103**, 124 (1999).
- [48] J. Vandevondele and J. Hutter, Gaussian basis sets for accurate calculations on molecular systems in gas and condensed phases, *The Journal of Chemical Physics* **127**, 114105 (2007).
- [49] G. J. Martyna, M. L. Klein, and M. Tuckerman, Nosé-hoover chains: The canonical ensemble via continuous dynamics, *J. Chem. Phys.* **97**, 2635 (1992).
- [50] S. Grimme, J. Antony, S. Ehrlich, and H. Krieg, A Consistent and Accurate Ab Initio Parametrization of Density Functional Dispersion Correction (DFT-D) for the 94 Elements H-Pu, *J. Chem. Phys.* **132**, 154104 (2010).
- [51] P. Virtanen, , R. Gommers, T. E. Oliphant, M. Haberland, T. Reddy, D. Cournapeau, E. Burovski, P. Peterson, W. Weckesser, J. Bright, S. J. van der Walt, M. Brett, J. Wilson, K. J. Millman, N. Mayorov, A. R. J. Nelson, E. Jones, R. Kern, E. Larson, C. J. Carey, Í. Polat, Y. Feng, E. W. Moore, J. VanderPlas, D. Laxalde, J. Perktold, R. Cimrman, I. Henriksen, E. A. Quintero, C. R. Harris, A. M. Archibald, A. H. Ribeiro, F. Pedregosa, and P. van Mulbregt, SciPy 1.0: fundamental algorithms for scientific computing in python, *Nature Methods* **17**, 261 (2020).